Geophys. J. Int. (2009) **177,** 451–462 doi: 10.1111/j.1365-246X.2009.04078.x

Subsidence and crustal roughness of ultra-slow spreading ridges in the northern North Atlantic and the Arctic Ocean

Birte-Marie Ehlers and Wilfried Jokat

Alfred Wegener Institute for Polar and Marine Research, Am Alten Hafen 26, 27568 *Bremerhaven, Germany. E-mail: Birte-Marie.Ehlers@awi.de*

Accepted 2008 November 26. Received 2008 November 3; in original form 2007 June 14

SUMMARY

Five basin-wide seismic reflection profiles of up to 550 km each were acquired in the Arctic Ocean and the northern North Atlantic in 2001 and 2002. The main objective was to investigate the depth to the basement and to analyse the crustal structure, morphology and roughness of ultra-slow spreading ridges of the Gakkel, Molloy and Knipovich ridges. To date, little is known to date of the ultra-slow spectrum of such spreading ridges. The seismic profiles of all investigated ridges show similar morphological characteristics with deep axial valleys and rough basement topography. Magnetic data compilation and interpretation suggests that the ultra-slow spreading systems are fairly stable and existed during the entire evolution of the basins to the north of the Greenland Fracture Zone. The thermal subsidence curve was calculated and corrected for sediment loads, and crustal roughness values are estimated for all five profiles. The resulting roughness values append the global roughness data set for ultra-slow spreading systems. The results are higher than those predicted by interpolating existing global roughness.

This study confirms the presence of a global relationship between crustal roughness, ridge morphology and spreading rates. New curve fits, supporting the global relationship, are discussed. Data on present spreading rates, ridge morphology, subsidence and roughness provide a better insight into the development of the axial ridge morphology in the study area. The results show that the basins to the north of the Greenland Fracture Zone were formed at ultra-slow spreading axial rift valleys and continued spreading at ultra-slow rates to the present day configuration.

Key words: Marine magnetics and palaeomagnetics; Sedimentary basin processes; Arctic region; Atlantic Ocean.

1 INTRODUCTION

Several methods have been used in the past to classify oceanic spreading rates and centres. One approach is to categorize mid-ocean ridge processes based on calculation of root mean square (rms) crustal roughness. In this context, roughness implies an indirect record of axial morphology and can provide observational constraints on the nature of changes in axial morphology, crustal thickness and tectonics (Ma & Cochran 1997).

The relationship between subsidence and age has been known for many years (Parsons & Sclater 1977). In recent years, several studies have compared crustal roughness values with ridge parameters such as spreading velocity, crustal thickness, faulting, segmentation or ridge morphology (e.g. Malinverno & Cowie 1993; Small 1994; Goff *et al*. 1997; Minshull 1999). The existence of a relationship between spreading rate and roughness was first published by Menard (1967) and Sclater & Francheteau (1970).

Dick *et al.* (2003) point out that on the basis of various studies at faster spreading centres, mid-ocean ridges have been divided into fast spreading rates (80–180 mm y^{-1} full rate), intermediate spreading rates (55–70 mm y^{-1}) and slow spreading rates (less than 55 mm y^{-1}). Spreading ridges with full spreading rates of less than 20 mm y^{-1} are characterized as ultra-slow spreading ridges. Several ultra-slow spreading ridges are present in the Arctic, but these ridges remain poorly characterized.

Abyssal hill morphology results from a complex combination of tectonics (surface faulting) and constructional (volcanic) processes, which occur at or near the ridge axis (Goff *et al.* 1993). In particular, spreading ridges with a full rate of less than 20 mm y^{-1} change between volcanic activity and normal faulting of crustal blocks due to tectonic strain during drifting. This change causes the roughness of the basement surface (Louden *et al.* 1996).

MacDonald (1982) assumes that crustal morphology reflects the spreading velocity with slow spreading ridges characterized by a deep axial valley and fast spreading ridges, such as the East Pacific Rise, characterized by a central high. But ridge tectonics is not just a function of spreading rates. It also depends on the ridge geometry, the mantle composition and the thermal structure of the crust (Dick *et al.* 2003).

Based on observations and extrapolations of faster spreading ridges, on theoretical modelling of the melting processes and on the thermal structure of the crust, the Gakkel Ridge should have sparse

volcanism, as well as very limited hydrothermal activity, and low melting of the underlying mantle. However, Michael *et al.* (2003), divided the Gakkel Ridge into a 300 km-long central amagmatic zone, which lies between abundant, continuous volcanism to the west and large, widely spaced volcanism centres to the east. Furthermore, spreading velocity decreases towards the east whereas crustal thickness does not vary and is controlled by the magmatic activity along the ridge (Jokat & Schmidt-Aursch 2007).

As existing global roughness models lack data from ultra-slow spreading systems, analyses from the ultra-slow spreading systems at the Gakkel Ridge in the northern North Atlantic and Fram Strait, as well as the adjacent basins, are of special interest.

The calculation of crustal roughness along the Knipovich and Molloy ridges in the northern North Atlantic and along the Gakkel Ridge in the Arctic Ocean can provide an insight into their morphological evolution. In present configuration, these ridges have ultra-slow spreading rates and a deep axial morphology.

According to the classification of mid-ocean ridges (Dick *et al.* 2003), the Gakkel Ridge has been an ultra-slow spreading system since the formation of the first oceanic crust at magnetic chron 24 (54 Ma). The half spreading rates at the Gakkel Ridge varied between 3 and $\sim$10 mm y^{-1} during initial opening (Karasik 1968; Vogt *et al.* 1979). Half spreading rates decrease from 7.3 mm y^{-1} in the Fram Strait to 3.2 mm y^{-1} in the Laptev Sea (DeMets *et al.* 1994).

Age models of oceanic crust based on identifications of magnetic anomalies are used to predict tectonic models for the northern North Atlantic and the Arctic Ocean (Kristoffersen 1990; Lawver *et al.* 1990). They indicate that active seafloor spreading in the Arctic Ocean and the northern North Atlantic probably started during chron 24 (53 Ma) at the Gakkel Ridge (Vogt *et al.* 1979) and at the Mohns Ridge in the Norwegian–Greenland Sea (Talwani & Eldholm 1977; Eldholm *et al.* 1987). In between these two systems, seafloor spreading at the Knipovich Ridge started to propagate northward from chron 13 (33 Ma; Eldholm *et al.* 1990), whereas the onset of seafloor spreading at the Molloy Ridge took place in the Early Miocene (21 Ma). For the Norwegian–Greenland Sea and the Eurasian Basin, Brozena *et al.* (2003) identified magnetic isochrones for the Gammaa-5 grid (Verhoef *et al.* 1996). This identification is restricted to 11 isochrons between chrons 5 and 25. These models are rather speculative, especially due to the lack of data in the Arctic region.

This study presents new seismic data from the Arctic Ocean and northern North Atlantic (Boreas and Molloy basins; Fig. 1), refines age models derived from magnetic data and calculates crustal roughness values for ultra-slow spreading ridges. Based on the above parameters, it is possible to constrain ultra-slow spreading ridges in the Arctic Ocean and the northern North Atlantic for the first time and thereby provide a clearer picture of the geodynamic evolution of these oceanic basins.

2 DATA

2.1 Seismic reflection profiles

Five reflection profiles of the northern North Atlantic and Arctic Ocean were studied. The profiles 20020500 and 20020700 from the northern North Atlantic (Fig. 1) were acquired by RV Polarstern with a 24 L VLF airgun cluster and an 800 m streamer, during the expedition ARKXVIII/2 cruise in 2002 (Jokat 2003). In this contribution, we will not discuss the seismic data in the Boreas and Molloy basins in detail but limit the discussion only to the shape of the oceanic basement. Both seismic profiles were depth-migrated (FD-migration) using velocity information from sonobuoy wide-angle recordings. Two sonobuoys were deployed on profile 20020500 (CDP 5750 and 7300) and three sonobuoys on profile 20020700 (CDP 5100, 10700 and 15450). The acoustic velocity of *P* waves in the water is revealed as 1.48 km s^{-1}, in sediments as 1.8–3.2 km s^{-1} and for the top of the acoustic basement as 3.3 km s^{-1}, with an error of 0.2 km s^{-1}. Therefore, the depth-migration has an error of about 160 m for the position of the acoustic basement with a sediment thickness up to 2000 m. Because of the small number of deployed sonobuoys, the velocity model is interpolated along the profiles.

Profile 20020500 (Figs 1 and 2a) runs SE–NW, parallel to the Spitsbergen Fracture Zone and the Greenland Spitsbergen Sill, from the axial rift valley of the Molloy Ridge to the East-Greenland Shelf. The line crosses the ridge at 79°20′N, 003°44′E (Fig. 2a; CDP 1180). The water depth close to the ridge averages 2750 m, and a rough basement surface is observed over the entire profile length. The average relief is about 1000 m, with a maximum basement jump of 2000 m at about 79°38′N, 000°59E (Fig. 2a, CDP 3800). Northwest of this position, the basement deepens to an average depth of 4700 m. Here, 2000-m-thick sediments cover the basement, whereas the southeastern part is bare or only sparsely sedimented. On the northwestern part of the profile, the basement rises to 2500 m. Here, it is not clear if oceanic crust is still present, or if this part of the profile belongs to the continent–ocean transition zone. The axial rift valley of the Molloy Ridge lies at a depth of nearly 4000 m and is completely free of sediments.

Profile 20020700 (Figs 1 and 2b) crosses the entire Boreas Basin as well as the axial valley of the Knipovich Ridge at 76°05′N 007°13′E (CDP 705). The average water depth is 2600 m, and the basement surface is as rough as observed on profile 20020500. Near the axial rift valley, almost no sediments exist. In contrast to profile 20020500, there is no basement jump where the sediment cover starts. The sediments thicken more or less constantly toward the NE-Greenland shelf. The sediment thickness varies up to a maximum of 2000 m. The basement deepens continuously from southeast to northwest, except for a 1500 m high and 15 km wide basement ridge/seamount at 77°24′N, 000°02′E (Fig. 2b; CDP 10100). Northwest of this feature, the sediment thickness averages 2500 m over a basement at 5500–6000 m depth (77°46′N, 002°09′W; Fig. 2b; CDP 12800). Toward the NE-Greenland margin, basement shoals to 4500 m over a distance of 5000 m: a gradient of 30 per cent. On the westernmost part of the profile, the basement rises from 5000 to 2000 m. This area (Fig. 2b; CDP 12 000–15 000) is supposed to be the seaward termination of the continent–ocean transition zone.

The three seismic reflection profiles 20010100, 20010300 and 20010460 (Figs 1 and 3) are located in the Arctic Ocean (Jokat & Micksch 2004) and are used for a roughness study in the western Eurasia Basin. These profiles are aligned almost perpendicular to the Gakkel Ridge and were acquired with a 24 L airgun array and a short streamer (48 channels, 6.25 m group spacing, 300 m active section) together with the USCGC Healy, due to the dense sea ice cover in this region (Thiede 2002). The acoustic *P*-wave velocities for the profiles are described in Jokat & Micksch (2004).

Profiles 20010100 (Fig. 3a) and 20010460 (Fig. 3b) (Jokat & Micksch 2004) were shot in the Nansen Basin, and start north of the Svalbard continental margin. Profile 20010100 (Fig. 3a) reaches the axial valley of the Gakkel Ridge at approximately 85°36′N, 016°41′E (CDP 21100). The axial valley has a water depth of 4800 m. East of the ridge, the flank of the Gakkel Ridge shows

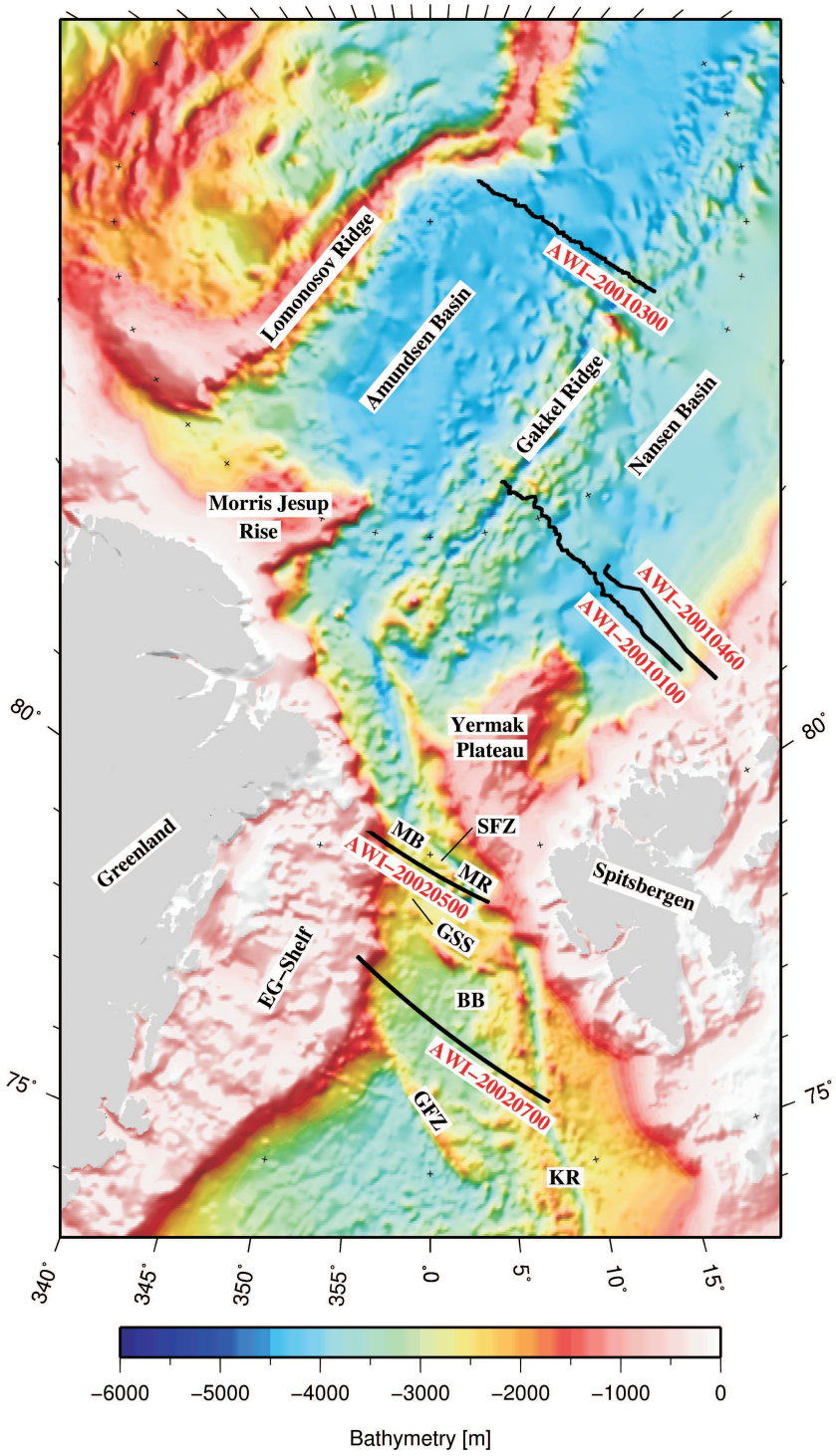

Figure 1. Bathymetry map of the international bathymetric chart of the Arctic Ocean (IBCAO; Jakobsson *et al.* 2001). The black lines show the seismic reflection profiles AWI-2001000, AWI-20010300 and AWI-20010460 in the Arctic Ocean and AWI-20020500 and AWI-20020700 in the northern North Atlantic, close to the Molloy Ridge (MR) and in the Boreas Basin (BB). KR, Knipovich Ridge; MB, Molloy Basin; SFZ, Spitsbergen Fracture Zone; GSS, Greenland Spitsbergen Sill and GFZ, Greenland Fracture Zone.

some pronounced basement highs around 85°13′N, 020°14′E (CDP 18000). In this area, the sediment cover is sparse or even absent. Southeast of a 1500 m high seamount at 84°43′N, 022°05′E (CDP 15000), the sediments continuously start to thicken towards the south. The water depth in the abyssal plain is about 4000 m. A seamount disrupts the sediment cover at 84°18′N, 022°39′E (CDP 12420), where the water depth shoals to 3710 m. The basement deepens down to 7500 m in the eastern part of the line.

The second profile in the Nansen Basin is line 20010460 (Fig. 3b; Micksch 2004). It is offset by 120 km to the east relative to line 20010100. Up to 3000 m of sediments overlie a basement surface with a relief of about 1000 m. The basement becomes shallower

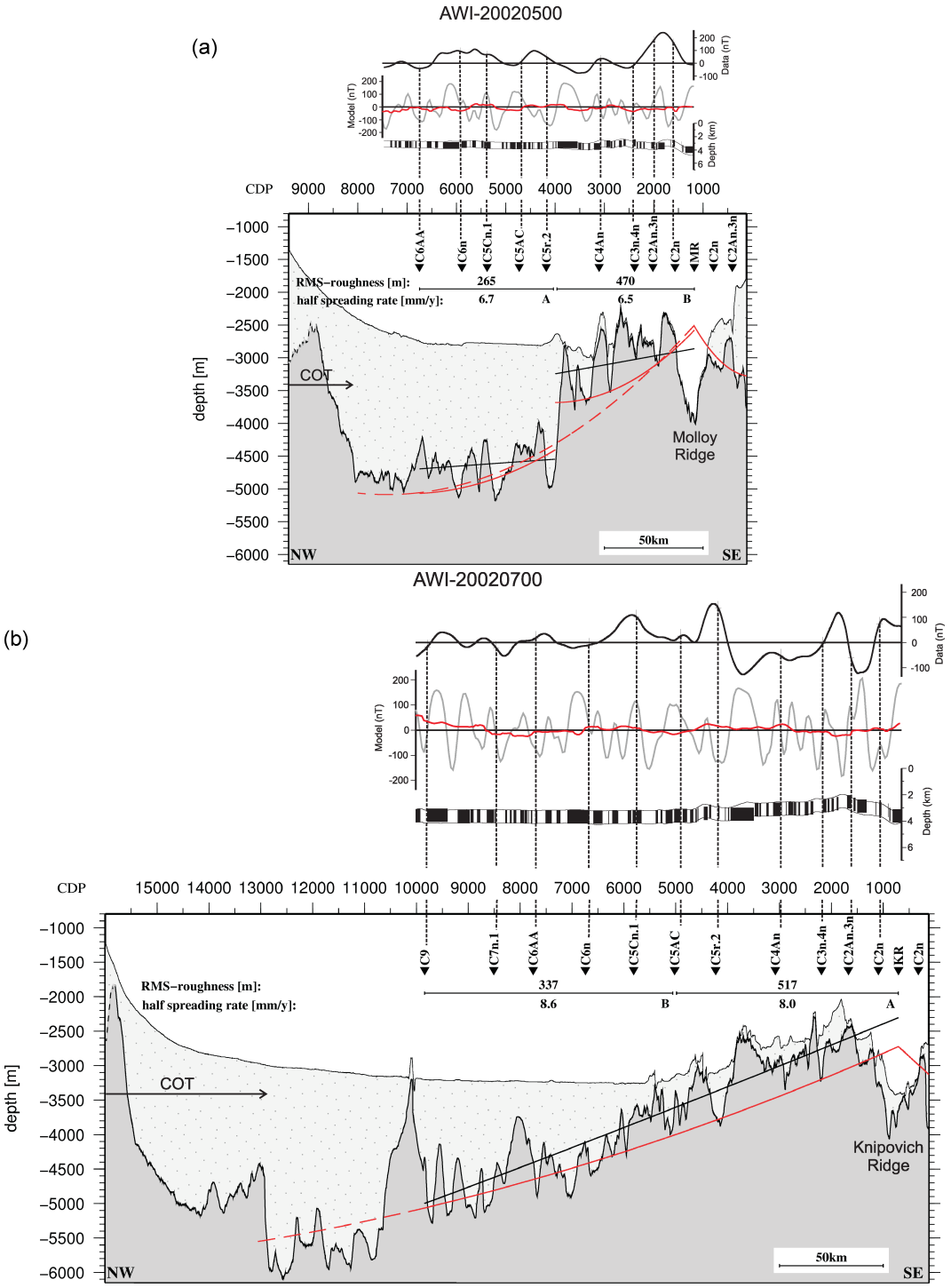

Figure 2. (a) Top: measured (black line), modelled (grey line) and filtered modelled magnetic data (red line) along profile AWI-20020500. Parameters for modelling: magnetic layer thickness 1 km; susceptibility $k = 0.0045$; inclination $I = 82.6^{\circ}$; declination $D = -5.9^{\circ}$; present day total intensity $F = 54453.8$ nT (after IGRF) and on-axis magnetization $J = 20$ A m^{-1}. Bottom: Line drawing of profile AWI-20020500 in the Molloy Basin crossing the Molloy Ridge (MR). Dark grey: basement; light and dotted grey: sediment cover. Red lines: thermal subsidence curve (southeastern part) and sediment-corrected subsidence curve (northwestern part). Dashed red line: subsidence curve for the whole oceanic crust northwest of the Molloy Ridge. Black line: empirical trend of basement depth used for rms roughness calculation. All seismic reflection profiles of Figs 2 and 3 are plotted in the same scale. COT, continent–ocean transition. (b) Top: Measured (black line), modelled (grey line) and filtered modelled magnetic data (red line) along profile AWI-20020500. Parameters for modelling: magnetic layer thickness 1 km; susceptibility $k = 0.0045$; inclination $I = 81.0^{\circ}$; declination $D = -2.5^{\circ}$; present day total intensity $F = 53771.51$ nT (after IGRF) and on-axis magnetization $J = 20$ A m^{-1}. Bottom: Line drawing of profile AWI-20020700 in the Boreas Basin crossing the Knipovich Ridge (KR). Dark grey: basement; light and dotted grey: sediment cover. Red line: thermal subsidence (close to the Knipovich Ridge) and sediment-corrected subsidence (basement with sediment covered) merged and fitted to one subsidence curve. Dashed red line: extrapolated subsidence curve. Black line: empirical trend of basement depth used for rms roughness calculation. COT, continent–ocean transition.

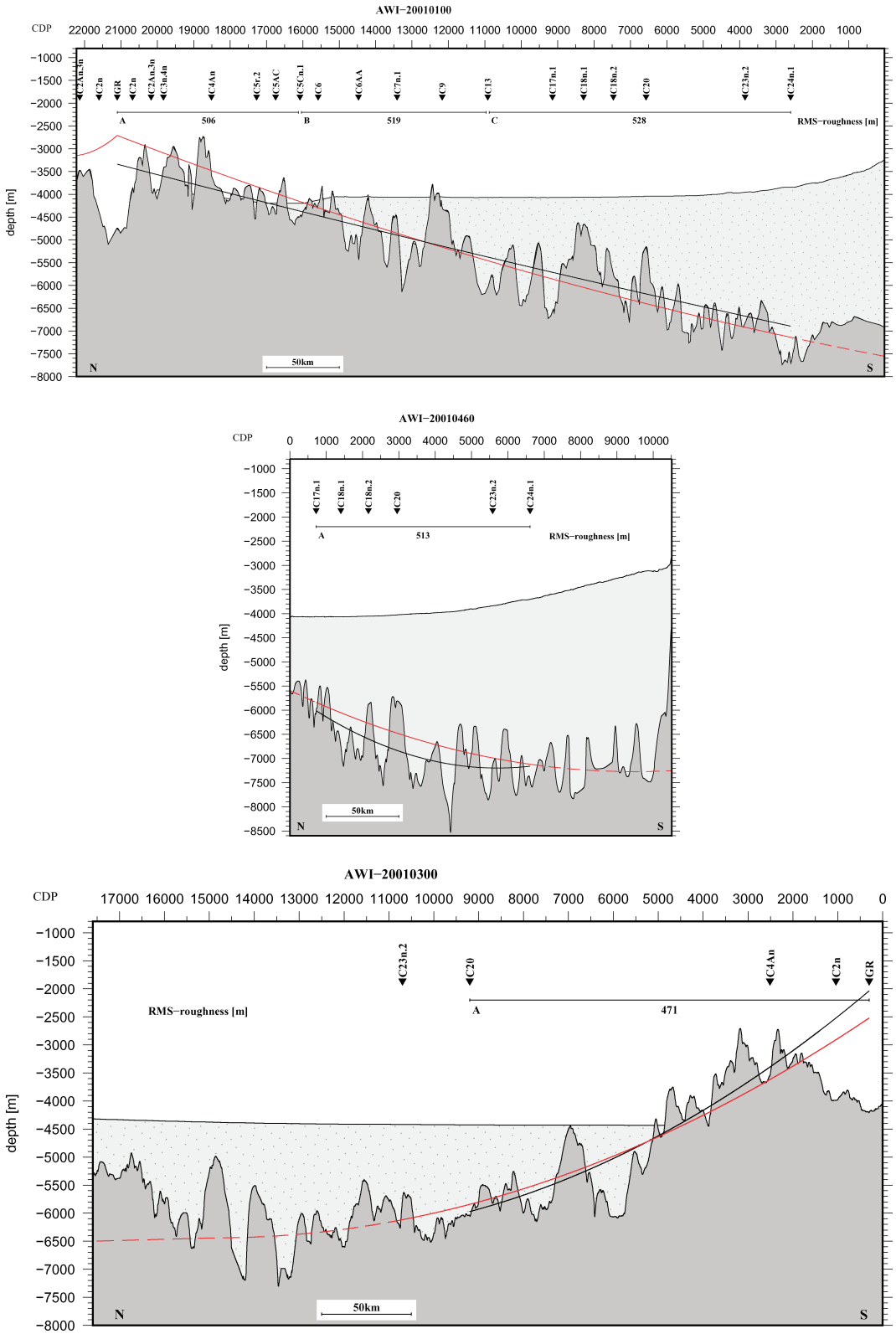

Figure 3. (a) Line drawing of the profile 20010100 in the Nansen Basin crossing the Gakkel Ridge (GR). Red line: sediment-corrected subsidence curve; dashed red line: extrapolated subsidence curve. Black line: empirical trend of basement depth used for rms roughness calculation, top: age model modified after Brozena *et al.* (2003). (b) Line drawing of the profile 20010460 in the Nansen Basin. Red line: sediment-corrected subsidence curve; dashed red line: extrapolated subsidence curve. Black line: empirical trend of basement depth used for rms roughness calculation. Top: age model modified after Brozena *et al.* (2003). (c) Line drawing of the profile 20010300 in the Amundsen Basin crossing the Gakkel Ridge (GR). Red line: sediment-corrected subsidence curve; dashed red line: extrapolated subsidence curve. Black line: empirical trend of basement depth used for rms roughness calculation. Top: age model modified after Brozena *et al.* (2003).

in the north (toward the Gakkel Ridge) and in the south (toward the Svalbard continental margin).

The seismic line 20010300 (Fig. 3c; Jokat & Micksch 2004) in the Amundsen Basin starts near 86°N at the Gakkel Ridge. From about 86°34′N, 073°53′E (CDP 1500) to 87°12′ N,077°50′ E (CDP 5000), the rough basement deepens from 3000 to 4500 m and has no sediment cover. North of this position, the basement drops by 2000 m over a distance of 15 km. From here on, the seismic reflection data show a sediment cover with a mean thickness of 1700 m, which continues to the foot of the Lomonosov Ridge. This sediment cover is disturbed by a seamount at 87°21′N 080°33′E (CDP 6900). A 7000 m deep basement low at 82°31′N, 099°40′E (CDP 13250) indicates the largest sediment thickness of the profile, before the basement depth shallows in the direction of the Lomonosov Ridge.

2.2 Magnetic data

Aeromagnetic data freely available for the region of the northern North Atlantic between the Greenland Fracture Zone and the Spitsbergen Fracture Zone were used for this study (GAMMAA5-Grid; Verhoef *et al.* 1996). The anomaly pattern in the Molloy and Boreas basins in this data set is mostly diffuse. Hence, new aeromagnetic data gathered by the Alfred Wegener Institute were used to supplement the existing surveys (Fig. 4; (Leinweber 2006). The helicopter survey was designed to follow the assumed spreading direction. Though, the overall magnetic anomaly field remained diffuse, a better resolution and hence identification of the anomalies was achieved in the Boreas and Molloy basins. The aeromagnetic anomalies in both data sets are more pronounced in the Boreas Basin than in the Molloy Basin.

3 ANALYSIS

The analysis consists of a calculation of the spreading rates based on a magnetic modelling and applies an age–depth relationship for subsidence calculations. Additionally roughness calculations are made.

3.1 Spreading rates

3.1.1 Method

Along the seismic reflection profiles, seafloor-spreading magnetic anomalies were re-identified based on identifications by Brozena *et al.* (2003) of magnetic anomalies at the Gakkel and Mohns ridges. Therefore, the 2-D magnetic modelling program MAGBATH (Hey *et al.* 1986) was used, and ages for the anomalies were determined according to the Geological Time Scale 2004 (Gradstein *et al.* 2004). The magnetic modelling consisted of varying estimated spreading

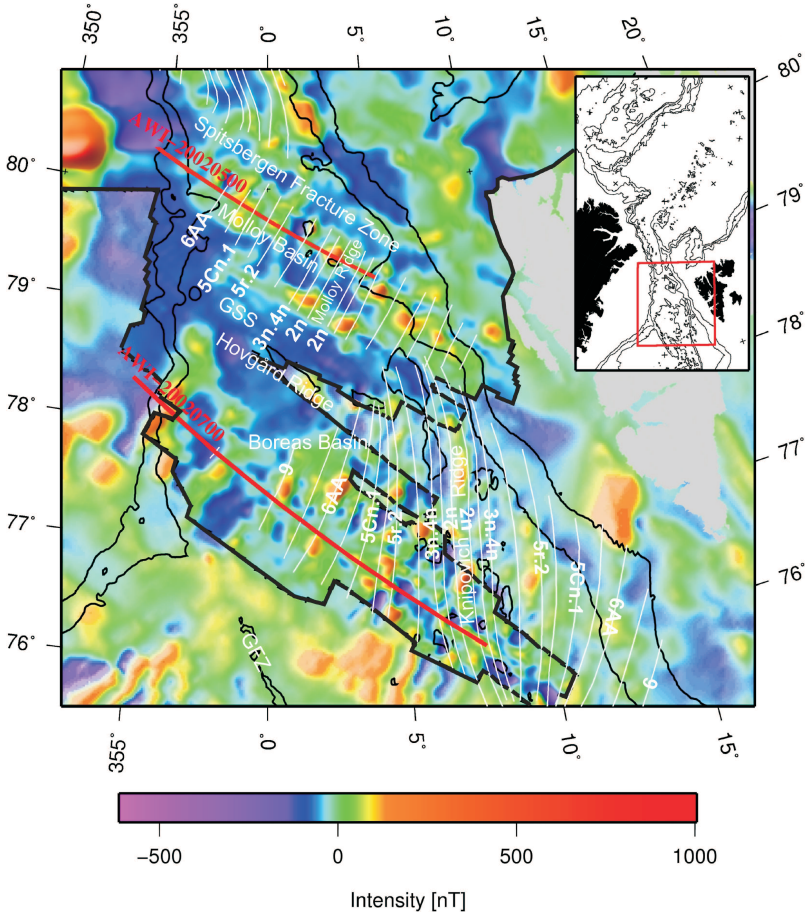

Figure 4. Age model for the Molloy and Knipovich ridges region. The white lines illustrate the re-identified magnetic chrons labelled after Gradstein *et al.* (2004). The seismic reflection profiles 20020500 and 20020700 are marked in red. The black line shows the limits of the new magnetic grid for the Fram Strait (Leinweber 2006). Additional magnetic data illustrated with lower intensity come from the GAMMAA5 grid (Verhoef *et al.* 1996). Thin black line: 1000 and 2000 m bathymetry contour line. GSS, Greenland Spitsbergen Sill and GFZ, Greenland Fracture Zone.

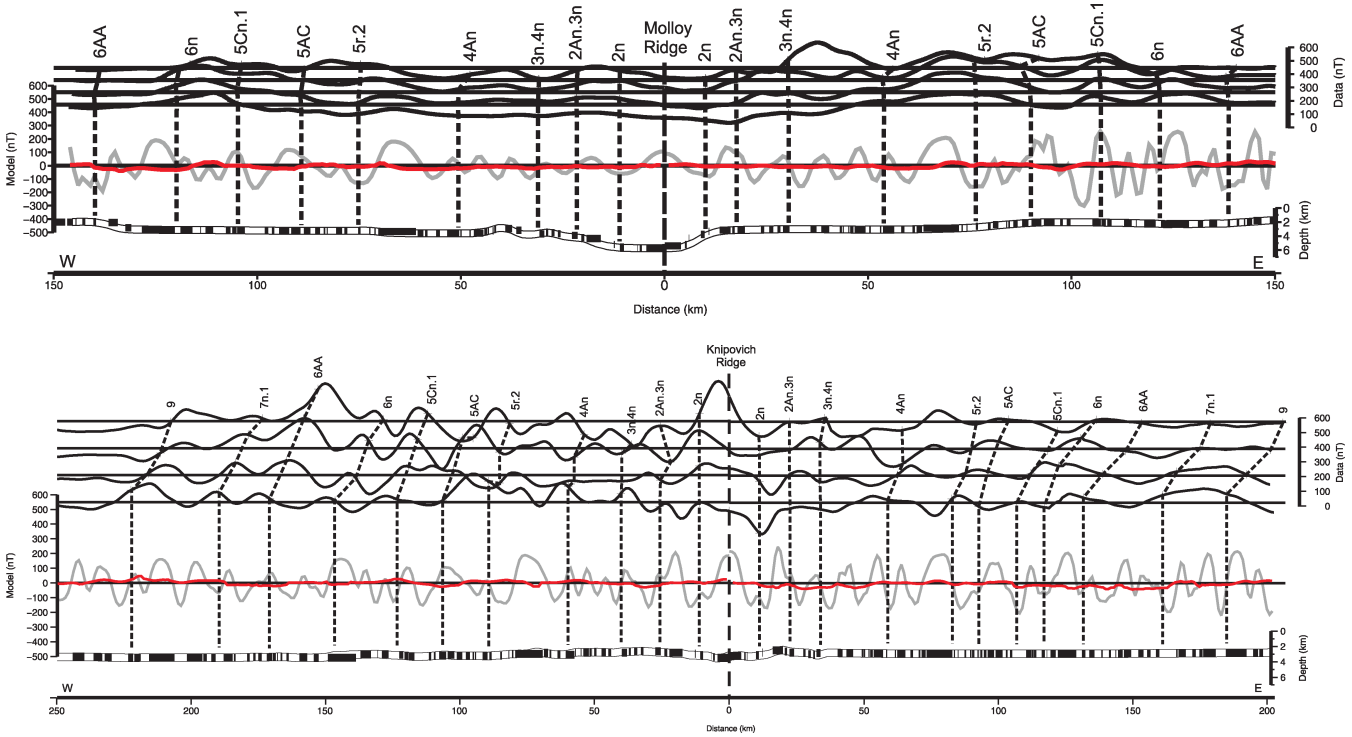

Figure 5. (a) Magnetic modelling of a helicopter survey 23 km south of profile 20020500 crossing the Molloy Ridge. The black line shows four measured profiles with a line spacing of 5 km, the grey line, the modelled data and the red line the filtered modelled data. At the bottom, the geomagnetic timescale after Gradstein *et al.* (2004) is presented. The re-identified isochrones are marked for a comparison of the measured and modelled data. (b) Magnetic modelling of a helicopter survey 27 km south of profile 20020700 crossing the Knipovich Ridge in the Boreas Basin. The black line shows four measured profiles with a line spacing of 10 km, the grey line, the modelled data and the red line, the filtered modelled data. At the bottom, the geomagnetic timescale after Gradstein *et al.* (2004) is presented. The re-identified isochrones are marked for a comparison of the measured and modelled data.

rates to obtain the best fits between measured and calculated anomalies. The assumed magnetic layer thickness, magnetic susceptibility, declination, inclination and the present-day total intensity are listed in Figs 2(a) and (b). For the identification of anomalies, an effort was made to avoid topographic elements impacting the analysis.

Since the aeromagnetic data do not show the most pronounced anomalies along the seismic lines (Figs 2a and b), transects 23 km south of line 20020500 (Fig. 5a) and 27 km south of line 20020700 (Fig. 5b) were used.

Four profiles in the vicinity of the above modelled lines were used to check the spatial continuity of the anomalies and their correct identification. The profiles have a line spacing of 5 km for the transect crossing the Molloy Ridge (Fig. 5a) and 10 km for the transect crossing the Knipovich Ridge (Fig. 5b).

Even though the resolution of the new aeromagnetic grid is substantially better, the magnetic anomalies presented in this data set are not as detailed as the calculated anomalies in the magnetic modelling. Comparing the modelled and measured anomalies, positive polarizations of the measured data include anomaly groups of the modelled data. Thus, we applied an appropriate filter to the computed anomalies from the model. Furthermore, some anomalies in the measured data are generated by topographic effects.

3.1.2 Results

The re-identified anomalies are presented in Fig. 4 (white lines). Whereas seafloor spreading at the Gakkel Ridge and in the Norwegian–Greenland Sea began during chron C24, at about 54 Ma (Brozena *et al.* 2003), seafloor spreading in the Molloy Basin started at about 21 Ma (during chron C6AA, this study); Fig. 4). The northern part of the Knipovich Ridge (east of the Hovgård Ridge) contains magnetic anomalies up to the beginning of chron C5 (10 Ma), whereas anomalies in the Boreas Basin can be clearly identified in the sequence up to chron C9 (28 Ma; Fig. 4).

The magnetic data grid (Fig. 4) shows that anomaly C9 east of the Knipovich Ridge is located just a few kilometres from the supposed continent–ocean transition zone off the Barents Sea, which corresponds to the 1000 and 2000 m bathymetry contour line. Anomaly C9 can probably be found in the Boreas Basin at 77°22′N, 000°15′E (Fig. 2b; CDP 9840) west of the Knipovich Ridge.

The basement lies at a depth of 5700 m northwest of the basement ridge/seamount at 77°24′N, 000°02′E (Fig. 2b; CDP 10100). If this great depth indicates the presence of oceanic crust, seafloor spreading might have started earlier than chron C9 (28 Ma).

Along profile 20020500, the half spreading rate was about 6.6 mm y^{-1} from the opening during chron 6AA (21 Ma) until today. Half spreading rates along line 20020700 started with 8.9 mm y^{-1} at chron 9 (28 Ma). Since 10 Ma, the oceanic crust accreted at an average half spreading rate of 6.2 mm y^{-1}. In the Arctic Ocean (line 20010100), half spreading rates for the Nansen Basin range from 7.5 mm y^{-1} at 54 Ma–33 Ma to 6.7 mm y^{-1} at 33 Ma–16 Ma and 6.0 mm y^{-1} at 16 Ma until the present. For the Amundsen Basin, the average half spreading rates of profile 20030300 is 4.7 mm y^{-1}. A spreading asymmetry between the Nansen and Amundsen basins first was reported by Vogt *et al.* (1979), who presented two curves for the northern and southern rift flank of the Gakkel Ridge with a difference in half spreading rates of 10–20 per cent.

In this study, half spreading rates east of the Molloy Ridge (0–12 Ma: 6.5 mm y^{-1}; 12–21 Ma: 6.3 mm y^{-1}) are similar to the values west of the ridge, whereas the rates at the Knipovich Ridge (0–14 Ma: 6.2 mm y^{-1}; 14–28 Ma: 6.4 mm y^{-1}) show an asymmetry of about 20–25 per cent, with higher rates on the western side.

3.2 Subsidence

3.2.1 Method

We applied the Parsons & Sclater (1977) age–depth relationship in combination with a sediment correction (Allen & Allen 1990) for the seismic reflection profiles 20010100, 20010300 and 20010460. The loading effect of the sediment is treated as a problem of local isostatic balance (Allen & Allen 1990). We applied the same formulae for profiles 20020500 and 20020700. For the area close to the ridge, where oceanic crust is quite young and only sparsely covered by sediments, thermal subsidence calculations (Parsons & Sclater 1977) were used to calculate the average basement depth. In areas with a large sediment cover, we corrected the subsidence curve for the sediment load (Allen & Allen 1990). The resulting values were fitted using quadratic regression (red solid lines, Figs 2 and 3).

In case of profile 20020500, we observed a significant basement jump (CDP 3800), and hence the profile was divided into two parts, which were treated separately.

The subsidence calculations for profiles 20010100, 20010300 and 20010460 use crustal ages based on the age model of Brozena *et al.* (2003) and on the GAMMAA5-Grid (Verhoef *et al.* 1996). For the subsidence analysis of profile 20020500 and 20020700, the age model based on the new geomagnetic data grid (Fig. 4; Leinweber 2006) is used, which was described in the previous section.

3.2.2 Results

The seismic reflection profiles in the Nansen, Amundsen, Molloy and Boreas basins show that the basement deepens as the oceanic crust ages and the sediment load increases (Figs 2 and 3). To correlate the observed as well as the theoretical basement depth, the calculated subsidence curves are shown in Figs 2 and 3. The dashed red lines show the extrapolated subsidence for the regions where age cannot be identified by magnetic anomalies, but where the depth of basement indicates oceanic crust.

All subsidence curves (Figs 2 and 3) based on the described age model fit the general trend of the basement as observed in the seismic reflection data. The mean deviation between the calculated subsidence and the empirical trend of the basement relief for all five profiles averages 244 m. The best fit achieves profile 20010300 with 119 m.

Especially, close to the axial rift valley of the Molloy and the Knipovich ridges, the oceanic crust is shallower than the theory predicts. This phenomenon is also observed on profile 20010300, close to the Gakkel Ridge. The basement surface in the northwestern part of profile 20020700 shows a good correlation to the extrapolated subsidence curve (dashed red line; Fig. 2b).

Assuming an error of 0.5 Myr for the age of the re-identified isochrones, the calculated subsidence values have an uncertainty of about 40 m.

3.3 Roughness

3.3.1 Method

Topographic roughness (R) is defined as the root mean square (rms) deviation of residual basement relief (h) along a given length of the profile (Malinverno 1991). The following equation is used for the calculation of R:

$$R_i = \sqrt{\sum_{i=1}^{n} \frac{h_i^2}{n}} \quad \text{for } i = 1, 2, \ldots, n, \tag{1}$$

in which h is the difference between a reference surface and the basement. The reference curve can be a straight line fit to the basement (Malinverno & Cowie 1993) or the theoretical subsidence curve (Hayes & Kane 1991). In this study, we used an empirical trend of the basement instead of the theoretical subsidence curves. Although the results of the theoretical subsidence reproduce the general trend of the basement, using the theoretical subsidence for roughness calculation biases the results, even after subtracting the square of mean value of the segment h from the variance. Another advantage of using an empirical trend of the basement as reference surface is that the roughness calculations are independent of the crustal age model.

The chosen length of the profile section should exceed some tens of kilometres, preferably about 100 km (Malinverno 1991), to overcome self-affinity problems and influences of window borders.

A power law derived from many measurements on oceanic ridge systems describing the relationship of roughness R and full spreading rate, v, is given by Malinverno (1991) as

$$R_C = 1296\ v^{-0.539}. \tag{2}$$

This power law only describes the relationship between rms roughness and spreading rate and does not consider the axial morphology. Goff *et al.* (1997) studied the statistical properties of abyssal hill morphology and showed that for identical spreading rates, both the axial morphology and the rms roughness change. Regarding this conclusion, separate power-law curves for axial valley-adjacent and axial high-adjacent values are calculated for this study as well.

For a roughness analysis, the empirical trends of the basement were calculated with an equal spacing of one CDP (25 m). Afterwards, we subtracted the basement depth values from the calculated empirical trend of basement depth to obtain the residual basement relief (h). R_i was calculated using eq. (1).

Profile sections were selected to calculate crustal roughness according to the knowledge of the crustal age or spreading rates, respectively, because spreading rates were not constant through time at all three ridges (this study). Therefore, the roughness calculation was done for separate intervals bounded by magnetic anomalies or the ridge axis. For profile 20020500, it was not possible to obtain interval borders further apart than 70 km because of a change in spreading rates at the basement jump at CDP 3800 (Table 1).

3.3.2 Results

The results of the roughness analysis are presented in Table 1. All new roughness values (this study) are calculated at ultra-slow spreading rates in ocean basins with axial rift valleys.

The rms roughness of all five axial valley-adjacent profiles (Table 1) located in the Arctic Ocean and the northern North Atlantic results in high roughness values from 265 m up to 528 m. The standard variation amounts to 93 m. Fig. 6 shows the relationship of the half spreading rate and the results of the roughness analysis

Table 1. Profile section, half spreading rates, age range, length of profile section, roughness, R_i, and predicted roughness, R_C, after the power law of Malinverno (1991) and after the power laws of this study, for the five profiles in the Arctic Ocean and northern North Atlantic.

	Section	Half-spreading rate (mm y^{-1})	Age range (Ma)	Length of profile section (km)	Roughnes R_i (m)	Roughness R_C (m) (Malinverno (1991))	Roughness R_C (m) (this study)
Nansen B.							
20010100	A	6.0	0–16	125	506	340	432
	B	6.7	16–33	127	519	320	405
	C	7.5	33–53	207	528	301	380
20010460	A	7.5	37–53	147	513	301	380
Amundsen B.							
20010300	A	4.7	0–42	223	471	387	497
Boreas/Molloy B.							
20020500	A	6.5	0–11	70	470	325	413
	B	6.7	11–21	68	265	320	405
20020700	A	8.0	0–14	107	517	291	366
	B	8.6	14–28	120	337	280	351

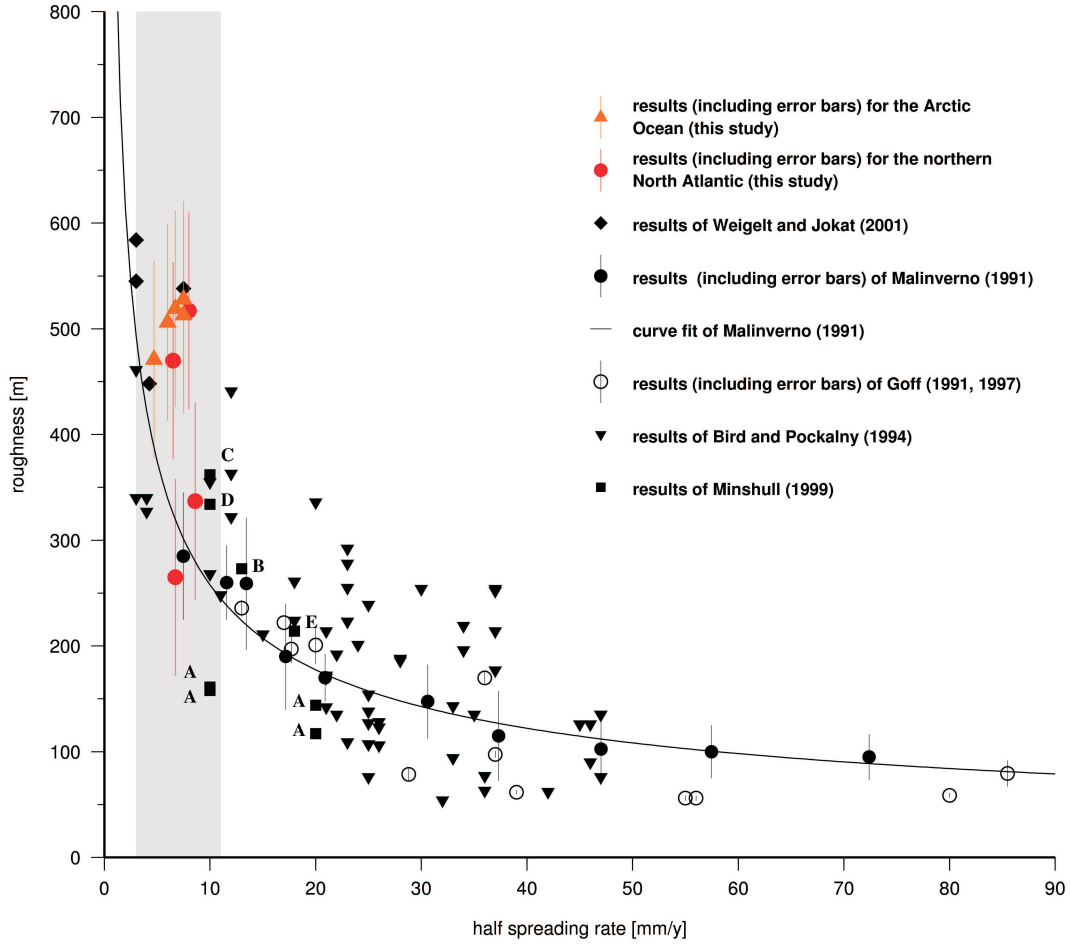

Figure 6. Roughness (m) versus half spreading rate (mm y^{-1}). The results of Goff (1991) and Goff *et al*. (1997) were obtained from the southern Mid Atlantic Ridge and the Pacific Ocean, the results of Bird and Pockalny (1994) from the South Australia Basin and the Argentine Basin. The roughness values of Minshull (1999) are from A: Blake Spur Fracture Zone (Morris *et al.* 1993), B: west flank of the Mid-Atlantic Ridge at 28°N, C: Canary Basin (Ranero *et al.* 1970), D: OCEANS area at the Cape Verde abyssal plain (Henstock & White 1996) and E: east flank of the Atlantic Ridge at the equator. The black line represents the curve fit of Malinverno (1991). The grey area marks the range of the half spreading rates for the Gakkel Ridge.

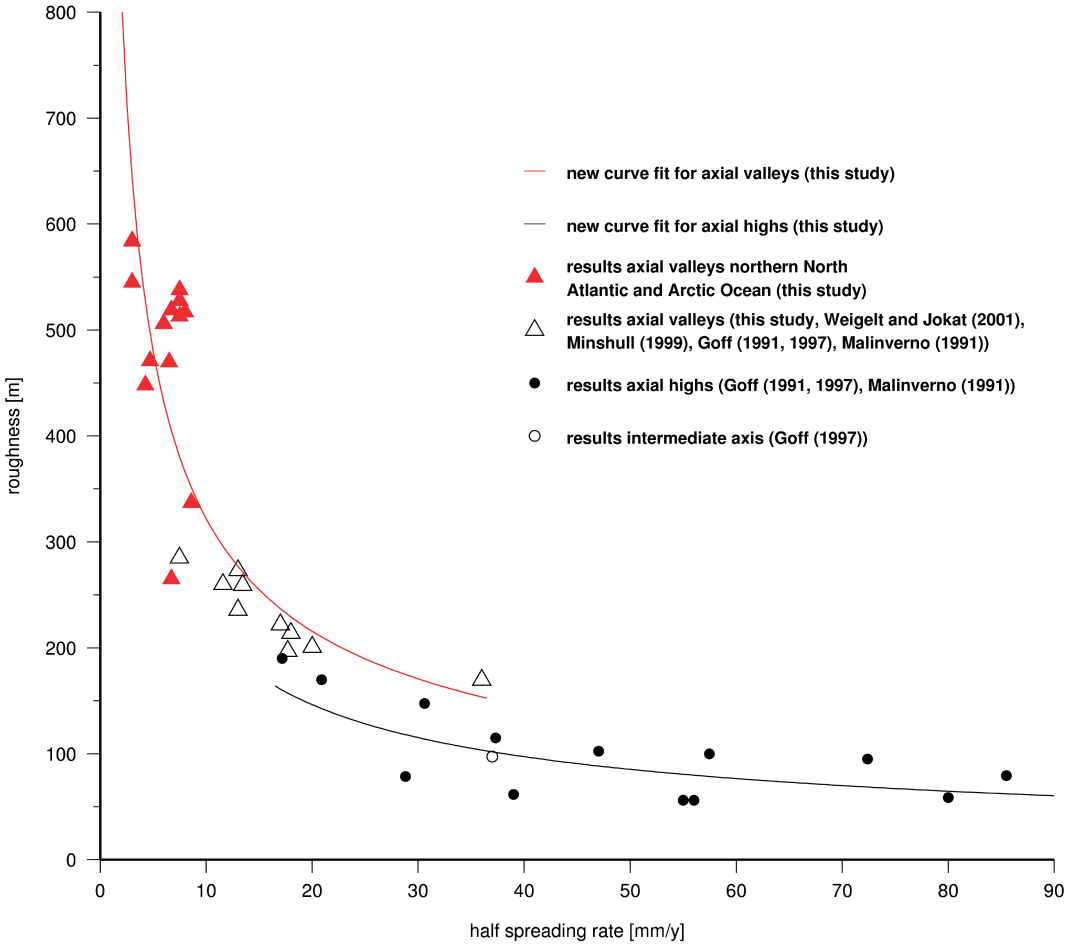

Figure 7. Roughness (m) versus half spreading rate (mm y^{-1}). The results of Goff (1991) and Goff *et al.* (1997), Malinverno (1991) and this study are separated in axial valley-adjacent, intermediate and axial high-adjacent roughness values. The red line represents the curve fit for axial valley-adjacent roughness values (this study), the black line shows the curve fit for axial high-adjacent roughness values (this study).

with the standard variation as error bars. The grey area marks the range of the ultra-slow spreading velocities for the Gakkel Ridge.

Fig. 7 presents data from axial valley-adjacent and axial high-adjacent roughness values. Especially for half spreading rates between 17 and 36 mm y^{-1}, both roughness values from axial rift valleys and axial rift highs exist. Therefore, based on the new roughness data, two separate power-law curve fits are calculated:

(1) for axial valley-adjacent values:

$$R_C = 1811\,(2v)^{-0.5767}\,; \tag{3}$$

(2) for axial high-adjacent values:

$$R_C = 1290\,(2v)^{-0.5898}\,. \tag{4}$$

The correlation coefficient is 0.86 for (3) and 0.71 for (4). The results of the various curve fits are shown in Fig. 7.

4 DISCUSSION

Seismic reflection data shows deep axial valleys and rough basement topography for all five profiles (Figs 2 and 3). Combining the results of the seismic reflection profiles and of the new aeromagnetic data grid (Fig. 4), an enhanced age model was developed. This age model, which is confirmed by magnetic modelling (Fig. 2a and b and 5a and b), suggests half spreading rates for all investigated basins to be located in the ultra-slow range, based on classification of mid-ocean ridges (Dick *et al.* 2003). Half spreading rates range from 6.0 to 8.6 mm y^{-1}.

For the Gakkel, Molloy and Knipovich ridges, the main reason for such ultra-slow spreading seems to be the slow absolute rates of motion of the bounding Eurasian and North American plates (Vogt *et al.* 1979). These plates are not undergoing significant subduction. Furthermore, the proximity of the ridges to the Euler pole of rotation (e.g. Gaina *et al.* 2002) also results in low angular velocities and, therefore, ultra-slow spreading. Ultra-slow spreading causes fast cooling of the asthenosphere, increasing the viscosity and lowering crustal production rates (Sleep & Rosendahl 1979).

The age–depth relationship of Parsons & Sclater (1977) in combination with a sediment correction (Allen & Allen 1990) was applied to the re-identified age model. The observed depth to basement can be explained by the thermal subsidence and the sediment loads. The theoretical subsidence curves (red lines, Figs 2 and 3) differ from the empirical trends of the basement (black lines, Figs 2 and 3) by up to 400 m. The uncertainty of the calculated subsidence curves can be attributed to errors in the age model of oceanic crust and in the sediment thickness derived from the seismic reflection data.

In Fig. 6, published roughness values (Ranero *et al.* 1970; Goff 1991, 1997; Bird & Pockalny 1994; Henstock & White 1996; Minshull 1999; Weigelt & Jokat 2001) are shown in a global

context, highlighting the relationship between crustal roughness and half spreading rates. The new roughness values supplement the global data for the ultra-slow end of the spectrum. The calculated roughness values for ultra-slow spreading rates range from 265 to 528 m. These are only dependent on the basement depth derived from seismic reflection data. The values are higher than roughness values derived from ridge-adjacent areas with higher spreading rates. The results support the global correlation of spreading rates and crustal roughness. The roughness values do not correlate with the magmatic and amagmatic segmentation (Michael *et al.* 2003) or the crustal thickness (Jokat & Schmidt-Aursch 2007), respectively.

With exception of the roughness value for the northwestern part of profile 20020500, all new roughness values worked on for the Fram Strait and the Arctic Ocean, including the ones by Weigelt & Jokat (2001), lie above the Malinverno (1991) curve fit. The roughness values of Bird & Pockalny (1994) are generally higher than the rms roughness data of Malinverno (1991) at ultra-slow spreading rates (<20 mm y^{-1}) but similar at intermediate rates (21–40 mm y^{-1}). The results of Goff (1991) and Goff *et al*. (1997) for intermediate and fast spreading rates lie under the Malinverno curve for most data points. The values for slow spreading rates lie above the curve. In general, the difference between roughness predictions from Malinverno (1991) and other authors increases as spreading rates decrease (Fig. 6). Most crustal roughness values result in higher values for slow spreading rates and in lower values for fast spreading rates. For spreading rates of 20 to 40 mm y^{-1}, the roughness values range about 100 m around the curve fit. Hence, a discussion regarding a new curve fit including the new roughness data is justified.

The error bars for the roughness calculations, which are displayed in Fig. 6, cannot account for the difference between the power-law curve fit (Malinverno 1991) and the roughness values. To specify the difference between crustal roughness values and the power-law fit, besides spreading rates and roughness values, the axial morphology is taken into account. Goff *et al.* (1997) divided the roughness analysis in values derived from axial rift valleys, intermediate rift axes and axial rift highs. If the ridge morphology is taken into account, the values calculated close to axial rift valleys are on average about 50 m higher than axial high-adjacent values (Fig. 7). We conclude that a single power law is not sufficient to predict the relationship between spreading rates and crustal roughness. A step-function relationship of half spreading rates and roughness may be a possible solution. The sharp increase of crustal roughness values for slow spreading rates and small changes in roughness for fast spreading rates determine the calculation of a polynomial relationship.

For axial valley-adjacent roughness values, the results of the power law (3) are higher than Malinverno (1991) predicts. The mean deviation adds up to 40 m. In contrast, the results of the curve fit of axial high-adjacent roughness values (4) are on average 23 m less than the calculated values of Malinverno's power law.

Identical morphology along ultra-slow spreading ridges thus provides roughness values of a wider range than along faster ridges. As an example, roughness values at 6.5–6.7 mm y^{-1} half spreading rate range over 254 m, from 265 to 519 m (Fig. 6, Table 1), whereas roughness values at 28.8–30.6 mm y^{-1} half spreading rate range over 69 m, from 79 to 148 m.

Eq. (3) was used to calculate roughness values R_C based on the estimated spreading rates (Table 1) from the re-identified isochrones in the Boreas Basin, Molloy Basin and in the Arctic Ocean. The rms roughness R_i (eq. 1) is on an average 55 m higher than R_C calculated after eq. (3) (this study) and 140 m higher than R_C calculated after Malinverno (1991) (eq. 2). Since the results of this study are derived from axial valley-adjacent roughness values, eq. (4) is only based on data from Goff (1991) and Goff *et al*. (1997) and Malinverno (1991). Using the existing database, just one roughness value with an intermediate axial morphology is available. Therefore, it is not possible to infer a relationship between intermediate axial morphology, roughness and spreading rate.

In this study, the high roughness values obtained from all five analysed seismic reflection profiles (Table 1) with ultra-slow seafloor spreading rates in the investigated basins with axial rift valleys indicate a correlation between spreading rate, axial morphology and roughness values. In the Arctic Ocean, Boreas Basin and at the Molloy Ridge, seafloor spreading was initiated at ultra-slow spreading rates and based on the age model, continues at slightly decreasing spreading velocities until today (Figs 2–4). The analysis of roughness shows higher roughness values during the entire evolution of the basins, and hence we conclude that the Gakkel, Molloy and Knipovich ridges have always been axial rift valleys.

5 CONCLUSIONS

The sediment-corrected thermal subsidence predicts the general trend of the observed basement depths in the Nansen, Amundsen, Boreas and Molloy basins. An exception occurs at the flanks close to the spreading centres, where the theoretical subsidence is larger than the measured basement depth.

The global data set of rms roughness has been updated with new values for ultra-slow spreading systems based on roughness calculations of seismic reflection profiles in the Arctic Ocean, the northern North Atlantic and Fram Strait.

The roughness values from basins with ultra-slow spreading rates and axial rift valleys derived in this study are higher than those predicted by the power law of Malinverno (1991). Furthermore, the axial valley-adjacent and axial high-adjacent roughness values were separated. Two curve fits describe the relationship of the seafloor spreading rate, the rms roughness and the ridge morphology.

All five seismic reflection profiles show the ridge as deep axial valleys and basins with rough basement topography. The new spreading rate model shows that all basins were formed at ultra-slow spreading rates and continued spreading at the same rate. For the investigated basins, a good correlation between spreading rate, morphology and roughness exists.

The results also indicate that the entire ocean floor north of the Greenland Fracture Zone was formed at ridges with axial rift valley morphology with ultra-slow spreading rates and continued to spread at these rates, creating a rough basement topography. This constant ultra-slow spreading rate during the formation and basin evolution is of special interest for future research in geodynamic and plate tectonics.

ACKNOWLEDGMENTS

We thank the captain and crew of RV Polarstern for their support and Tim Minshull, John Goff and Donna Shillington for their helpful reviews, which improved this manuscript much. Furthermore, thanks are given to Vikram Unnithan and Aysel Sorensen for improving the English of the manuscript.

REFERENCES

Allen, P.A. & Allen, J.R., 1990. *Basin Analysis Principles & Applications,* Blackwell Science Publications, Oxford, p. 272.

Bird, R.T. & Pockalny, R.A., 1994. Late Cretaceous and Cenozoic seafloor and oceanic basement roughness: spreading rate, crustal age and sediment thickness correlations, *Planet. Sci. Lett.,* **123,** 239–254.

Brozena, J.M., Childers, V.A., Lawver, L.A., Gahagan, L.M., Forsberg, R., Faleide, J.I. & Eldholm, O., 2003. New aerogeophysical study of the Eurasia Basin and Lomonosov Ridge: implications for basin development, *Geology,* **31,** 825–828.

DeMets, C., Gordon, R.G., Argus, D.F. & Stein, S., 1994. Effect of recent revisions to geomagnetic reversal time scale on estimates of current plate motions, *Geophys. Res. Lett.,* **21,** 2191–2194.

Dick, H.J.B., Lin, J. & Schouten, H., 2003. An ultraslow-spreading class of ocean ridge, *Nature,* 405–412.

Eldholm, O., Faleide, J.I. & Myhre, A.M., 1987. Continent-ocean transition at the western Barents Sea/Svalbard continental margin, *Geology,* **15,** 1118–1122.

Eldholm, O., Karasik, A.M. & Reksnes, P.A., 1990. The North American plate boundary, in *The Arctic Ocean region, Band L of The Geology of North America,* pp. 171–184, eds Grantz, A., Johnson, L. & Sweeney, J.F., Geological Society of America, Boulder, Colorado.

Gaina, C., Roest, W.R. & Müller, R.D., 2002. Late Cretaceous – Cenozoic deformation of northeast Asia, *Earth planet. Sci. Lett.,* **197,** 273–286.

Goff, J.A., 1991. A global and regional stochastic analysis of near-ridge abyssal hill morphology, *J. geophys. Res.,* **96**(B13), 21 713–21 737.

Goff, J.A., Malinvero, A., Fornari, D.J. & Cochran, J.R., 1993. Abyssal Hill segmentation: quantitative analysis of the East Pacific Rise Flanks 7°S-09°S, *J. geophys. Res.,* **98**(B8), 13 851–13 862.

Goff, J.A., Ma, Y., Shah, A., Cochran, J.R. & Sempéré, 1997, Stochastic analysis of seafloor morphology on the flank of the southeast Indian Ridge: the influence of ridge morphology on the formation of abyssal hills, *J. geophys. Res.,* **102**(B7), 15 521–15 534.

Gradstein, F., Ogg, J. & Smith, A. (eds), 2004. *A Geological Time Scale 2004,* Cambridge University Press, Cambridge.

Hayes, D.E. & Kane, K.A., 1991. The dependence of seafloor roughness on spreading rate, *Geophys. Res. Lett.,* **18**(8), 1425–1428.

Henstock, T.J. & White, R.S., 1996. Along-axis variability in crustal accretion at the Mid-Atlantic ridge: results from the OCEAN study, *J. geophys. Res.,* **B6**(101), 13 673—13 688.

Hey, R.N., Kleinrock, M.C., Miller, S.P., Atawater, T.M. & Searle, R.C., 1986. Sea Beam/Deep-Tow investigation of an oceanic propagating rift system, *J. geophys. Res.,* **91,** 3369–3393.

Jakobsson, M. & IBCAO Editorial Board Members, 2001. Improvement to the International Bathymetric Chart of the Arctic Ocean (IBCAO): updating the data base and the grid model, *EOS, Trans. Am. geophys Un.,* **82**(47), Fall Meet. Suppl., Abstract OS11B-0371.

Jokat, W. (ed.), 2003, The expedition ARKTIS XVIII/2 of RV "Polarstern" in 2002: contributions of the participants, Berichte zur Polar- und Meeresforschung, Alfred-Wegener-Institut fuer Polar-und Meeresforschung, Bremerhaven, p. 449.

Jokat, W. & Micksch, U., 2004. Sedimentary structure of the Nansen and Amundsen basins, Arctic Ocean, *Geophys. Res. Lett.,* **31**(2), 4pp.

Jokat, W. & Schmidt-Aursch, M.C., 2007. Geophysical characteristics of the ultraslow spreading Gakkel Ridge, Arctic Ocean, *Geophys. J. Int.,* **168,** 983–998.

Karasik, A.M., 1968. Magnetic anomalies of the Gakkel Ridge and origin of Eurasian subbasin of the Artic Ocean, *Geophys. Methods Prospect. Arctic,* **5,** 8–19.

Kristoffersen, Y., 1990. On the tectonic evolution and palaeoceanographic significance of the Fram Strait gateway, in *Geological History of the Polar Oceans: Arctic Versus Antarctic,* pp. 63–76, eds Bleil, U. & Thiede, J., Kluwer Academic Publishers, Bremen.

Lawver, L.A., Müller, R.D., Srivastava, S.P. & Roest, W., 1990. The opening of the Arctic Ocean, in *Geological History of the Polar Oceans: Arctic Versus Antarctic,* pp. 29–62, eds Bleil, U. & Thiede, J., Kluwer Academic Publishers, Bremen.

Leinweber, V.T., 2006. Abschätzung von Sedimentmächtigkeiten in der Framstraße anhand magnetischer Daten, *Diploma thesis*. Karl-Franzens-University, Graz, 96pp.

Louden, K.E., Osler, J.C., Srivastava, S.P. & Keen, C.E., 1996. Formation of oceanic crust at slow spreading rates: new constraint from an extinct spreading center in the Labrador Sea, *Geology,* **24**(9), 771–774.

Ma, L.Y. & Cochran, J.R., 1997. Bathymetric roughness of the Southeast Indian Ridge: implications for crustal accretion at intermediate spreading rate mid-ocean ridges, *J. geophys. Res.,* **102**(B8), 17 697–17 711.

MacDonald, K.C., 1982. Mid-ocean ridges: fine scale tectonic, volcanic and hydrothermal processes within the plate boundary zone, *Ann. Rev. Earth planet. Sci.,* **10,** 155–190.

Malinverno, A., 1991. Inverse square-root dependence of mid-ocean ridge flank roughness on spreading rate, *Nature,* **352,** 58–60.

Malinverno, A. & Cowie, P.A., 1993. Normal faulting and the topographic roughness of mid-ocean ridge flanks, *J. geophys. Res.,* **98**(B10), 17 921–17 939.

Menard, H.W., 1967, Sea-floor spreading, topography, and the second layer, *Science,* **157**(3791), 923–924.

Michael, P.J. *et al*., 2003. Magmatic and amagmantic seafloor generation at the ultraslow-spreading Gakkel ridge, Arctic Ocean, *Nature,* **423,** 956–961.

Micksch, U., 2004. Sedimentary structure, subsidence history roughness analysis of Nansen and Amundsen Basin, Arctic Ocean, *Diploma thesis*. University of Karlsruhe, Karlsruhe.

Minshull, T.A., 1999. On the roughness of Mesozoic oceanic crust in the western North Atlantic, *Geophys. J. Int.,* **136,** 286–290.

Morris, E., Detrick, R.S., Minshull, T.A., Mutter, J.C., White, R.S., Su, W. & Buhl, P., 1993. Seismic structure of oceanic crust in the western North Atlantic, *J. geophys. Res.,* **98,** 13 879–13 903.

Parsons, B. & Sclater, J.G., 1977. An analyses of the variation of ocean floor bathymetry and the heat flow with age, *J. geophys. Res.,* **82**(5), 803–827.

Ranero, C.R., Banda, E. & Buhl, P., 1970. The crustal structure of the Canary Basin: accretion process at slow spreading centres, *J. geophys. Res.,* **102**(B5), 10 185–10 201.

Sclater, J.G. & Francheteau, J., 1970. The implications of terrestrial heat flow observations on current tectonic and geochemical models od the crust and upper mantle of the earth, *Geophys. J. R. astron. Soc.,* **20,** 509–542.

Sleep, N.H. & Rosendahl, B.R., 1979. Topography and tectonics of mid-ocean ridge axis, *J. geophys. Res.,* **84**(B12), 6831–6839.

Small, C., 1994. A global analysis of mid-ocean ridge axial topography, *Geophys. J. Int.,* **116,** 64–84.

Talwani, M. & Eldholm, O., 1977. Evolution of the Norwegian-Greenland Sea, *Geol. Soc. Am. Bul.,* **88,** 969–999.

Thiede, J. & the Shipboard Scientific Party, 2002. POLARSTERN ARKTIS XVII/2, Cruise Report: AMORE 2001 (Arctic Mid-Ocean Ridge Expedition), Berichte zur Polar- und Meeresforschung, Alfred-Wegener-Institute fuer Polar-und Meeresforschung, Bremerhaven, p. 421.

Verhoef, J., Macnab, R., Roest, W., Arjani-Hamed, J. & the project team, 1996. Magnetic anomalies of the Arctic and North Atlantic and adjacent land areas: GAMMAA5 (Gridded Aeromagnetic and Marine Magnetics of the North Atlantic and Arctic, 5 km), Open File 3125a (CD-Rom), Geological Survey of Canada.

Vogt, P.R., Taylor, P.T., Kovacs, L.C. & Johnson, G.L., 1979. Detailed aeromagnetic investigations of the Arctic Basin, *J. geophys. Res.,* **84,** 1071–1089.

Weigelt, E. & Jokat, W., 2001. Peculiarities of roughness and thickness of oceanic crust in the Eurasian Basin, Arctic Ocean, *Geophys. J. Int.,* (145), 505–551.